AGU ADVANCING EARTH AND SPACE SCIENCES

Geophysical Research Letters

RESEARCH LETTER
10.1029/2025GL119079

The Zonal Wave-3 Mode Impacts Antarctic Dense Water Formation

M. Auger[1,2,3], **P. Spence**[1,2,4,5], **and A. K. Morrison**[6]

[1]Institute for Marine and Antarctic Studies, University of Tasmania, Nipaluna/Hobart, TAS, Australia, [2]The Australian Centre for Excellence in Antarctic Science, University of Tasmania, Nipaluna/Hobart, TAS, Australia, [3]Laboratoire d'Océanographie Physique et Spatiale, University of Brest, CNRS, Ifremer, IRD, IUEM, Plouzané, France, [4]The Australian Antarctic Partnership Program, University of Tasmania, Nipaluna/Hobart, TAS, Australia, [5]The Australian Centre of Excellence for Weather of the 21st Century, University of Tasmania, Nipaluna/Hobart, TAS, Australia, [6]Research School of Earth Sciences and Australian Centre for Excellence in Antarctic Science, Australian National University, Canberra, ACT, Australia

Key Points:

- A perturbation simulation shows that the Zonal Wave-3 mode has a large impact on dense water formation
- Sea ice formation and salinity on the Ross and Weddell continental shelves are impacted differently by the same Zonal Wave-3 mode phases
- The signature of the Zonal Wave-3 mode on dense water formation can be found in simulations forced by the historical atmospheric record

Supporting Information:

Supporting Information may be found in the online version of this article.

Correspondence to:

M. Auger,
matthis.auger@univ-brest.fr

Citation:

Auger, M., Spence, P., & Morrison, A. K. (2026). The Zonal Wave-3 mode impacts Antarctic dense water formation. *Geophysical Research Letters*, *53*, e2025GL119079. https://doi.org/10.1029/2025GL119079

Received 5 SEP 2025
Accepted 1 JAN 2026

Abstract

At the Antarctic margins, dense water masses form as sea ice develops, driving the Antarctic branch of the global meridional overturning circulation. Previous studies found that large-scale climate modes such as the Southern Annular Mode and El Niño Southern do not fully account for the interannual variability of dense water formation. Here, we investigate the influence of the overlooked Zonal Wave-3 (ZW3) mode, characterized by three alternating cyclone–anticyclone pairs in the Southern Hemisphere mid-latitudes. Simulations with ZW3 perturbations of different phases show multi-year impacts on dense water formation and export. The PC1 phase exerts the strongest influence in the Ross Sea, while the PC2 phase can nearly shut down or double dense water formation in the Weddell Sea. A simulation with interannually varying atmospheric forcing confirms ZW3 correlates with dense water formation in both regions. Our results highlight that ZW3 is a key driver of Antarctic dense water dynamics.

Plain Language Summary

At the edges of Antarctica, interactions between the atmosphere, ocean, and sea ice create very cold, dense waters on the continental shelf. These waters sink and flow into the deep ocean, carrying nutrients, heat, and carbon with them. The amount of water formed and exported varies greatly from year to year at the four main formation sites, but previous studies have found only weak links to large-scale atmospheric patterns. Here, we show that variability in the Zonal Wave-3 mode—an atmospheric pattern made up of three pairs of cyclones and anticyclones circling the Southern Hemisphere—does influence these deep ocean currents. Our model simulations reveal that the formation and export of dense waters over multiple years depends strongly on the strength and position of this atmospheric pattern.

1. Introduction

At the Antarctic coast, open polynyas form where winds and currents promote sea ice divergence (Nihashi & Ohshima, 2015). These openings expose near-freezing surface waters to the atmosphere, enabling intense heat loss and rapid sea-ice production, with newly formed ice advected away by the prevailing winds (Morales Maqueda et al., 2004). The associated brine rejection generates Dense Shelf Water (DSW), which spreads across the continental shelf, overflows the shelf break, and descends the slope to renew Antarctic Bottom Water. Interannual variability in DSW formation can arise from changes in winds and sea-ice conditions (Schmidt et al., 2023; Silvano et al., 2020). Atmospheric forcing can either enhance or suppress polynyas activity, thereby promoting or reducing DSW production. Links between DSW variability and large-scale climate modes remain unclear. In simulations, Prydz Bay is the only region where DSW formation has been correlated with the Southern Annular Mode: its positive phase weakens the coastal easterlies, reducing sea-ice import and favoring polynya development (Schmidt et al., 2023). Similar polynya-enhancing effects during extreme El Niño events have been reported in the Ross Sea (Silvano et al., 2020). In the Weddell Sea, the Interdecadal Pacific Oscillation and Amundsen Sea Low have been associated with northerly wind anomalies that suppress polynya activity and slow DSW formation (Zhou et al., 2023). However, observational records of interannual DSW variability remain sparse, and these limitations constrain the robustness of current conclusions.

Here we evaluate the role of the Zonal Wave-3 (ZW3) mode in modulating DSW formation and export. ZW3 is the leading meridional wind anomaly mode over the Southern Ocean, expressed as three cyclone–anticyclone

10.1029/2025GL119079

pairs (Raphael, 2004). A new ZW3 index capturing magnitude and phase (Goyal et al., 2022) has revealed phase shifts important for Southern Ocean climate, including sea-ice dynamics (Eabry et al., 2024; Goyal et al., 2022), the 2016 sea-ice decline (Meehl et al., 2019; Purich & England, 2019; Purich et al., 2018; Schlosser et al., 2018; Wang et al., 2019), and the 2023 minimum (Jena et al., 2024). Despite its known impact on wind and sea ice, ZW3's influence on Antarctic shelf waters is largely unstudied. As wind and sea ice drive interannual DSW variability, understanding the role of the ZW3 climate mode in the variability of the Antarctic meridional overturning circulation is key, especially as the Southern Hemisphere atmosphere trends toward a more ZW3-like pattern (Schroeter et al., 2023). Its asymmetric winds suggest regionally distinct responses in the Ross Sea, Weddell Sea, Prydz Bay, and Adélie Land, which are the main contributors of DSW.

2. Methods and Data

2.1. ACCESS-OM2-01 Simulation

We use the Australian Community Climate and Earth-System Simulator Ocean Model (Kiss et al., 2020, ACCESS-OM2-01), a global ocean–sea ice model with 0.1° horizontal resolution (approximately 4 km at the continental shelf break) and 75 vertical z* levels, based on the ocean model MOM5.1 (Griffies, 2012) and coupled to the CICE5.1.2 sea ice model (Hunke & Lipscomb, 2010). The model excludes ice shelf cavities and tides, is forced by JRA55-do reanalysis (Tsujino et al., 2018), and restores surface salinity to a World Ocean Atlas climatology (Kiss et al., 2020).

Two baseline simulations are used. The historical run (1958–2018) assesses DSW interannual variability under realistic interannually varying atmospheric forcing. We use the third cycle of this simulation under the same atmospheric forcing but with different initial conditions. In contrast, the CONTROL run is forced by a single year of atmospheric forcing (May 1990–April 1991). The CONTROL run was equilibrated for 280 years and concomitantly extended with the perturbation experiments, providing a steady baseline to compare with perturbation simulations. The Repeat Year Forcing (RYF) of the CONTROL simulation was chosen for its relatively neutral state across all major climate indices (Stewart et al., 2020). ACCESS-OM2-01 realistically simulates dense water formation in Antarctic polynyas (Morrison et al., 2020), though export in Prydz Bay may be under-resolved (Mensah et al., 2021).

2.2. ZW3 Perturbations

The ZW3 perturbation reproduce the effect of strong ZW3 phases on atmospheric forcing. Perturbation anomalies are derived from the two leading EOFs of 500 hPa meridional wind (Goyal et al., 2022). These EOFs are computed using winds from the JRA55 reanalysis, with minimal differences to the ERA5-derived EOFs of Goyal et al. (2022) (Figure S1 in Supporting Information S1). The four ZW3 phases (0°, 90°, 180°, 270°) correspond to the positive and negative polarities of PC1 and PC2 (PC1±, PC2+±).

Perturbations for each of the CONTROL simulation forcing fields (sea-level pressure, 10-m winds, surface air temperature, humidity, precipitation, and radiation) are constructed independently for each calendar month. For a given month, we regress the interannual variability of each forcing field at each grid point onto the corresponding monthly PCs. The mean 10-m meridional wind perturbation and sea-level pressure obtained from these regressions are shown Figures 1a and 1b. As computation restrictions prevent us from modeling the full range of strengths of the ZW3 pattern, the perturbations used here aim to hit the model with strong ZW3 events to show the upper bound of the sensitivity. The resulting regression patterns are therefore scaled to match the 10% strongest positive or negative ZW3 events, yielding a monthly average perturbation anomaly (Figures 1c and 1d), linearly interpolated to 3-hourly resolution and added to the CONTROL forcing to retain synoptic-scale variability. The interpolation step introduces only minimal error, as the perturbations vary smoothly in time and represent monthly anomalies rather than high-frequency signals.

These perturbations are branched off the 280 years long CONTROL simulation with repeat-year forcing. The perturbations are applied for 1 year, then switched off to also investigate lagged responses for a further 3 years. Because most ZW3 variability occurs on sub-annual timescales, with PC1 and PC2 spectra peaking at 10–12 months (Figure S2 in Supporting Information S1), a 1-year perturbation corresponds to a "sustained" ZW3 pattern—that is, the long end of typical ZW3 persistence. The strongest perturbations occur in the West Antarctic, Weddell and Ross sectors (Figures S3–S4 in Supporting Information S1), consistent with the spatial amplitude

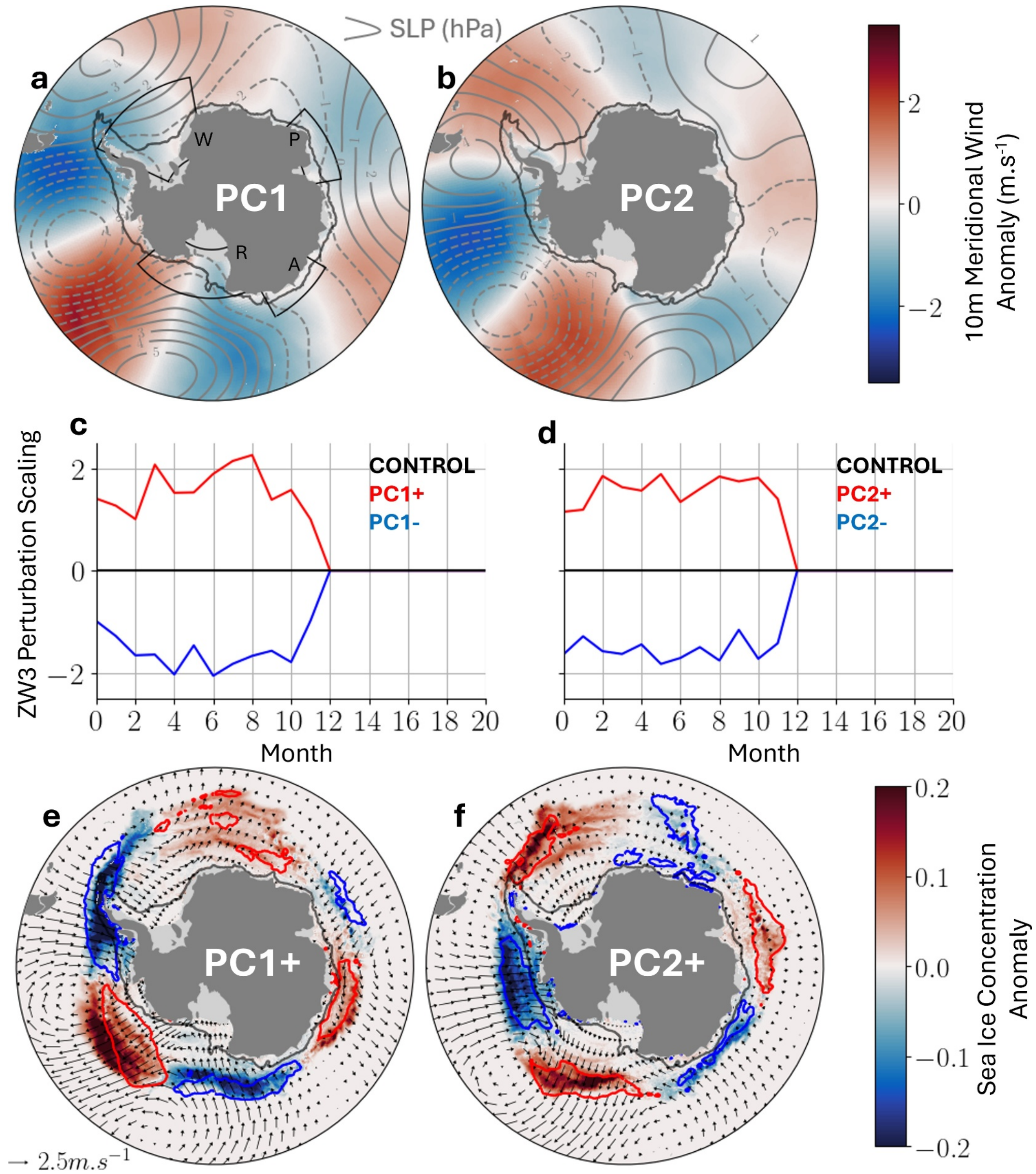

Figure 1. ZW3 perturbation experiments and dense water formation response. (a–b). Mean spatial pattern of the meridional wind (background color) and sea level pressure perturbations anomalies (gray contours) for PC1+ and PC2+. The black contour is the 1000 m isobath. The black regions indicate the main dense water formation discussed here (W: Weddell Sea, R: Ross Sea, P: Prydz Bay, A: Adélie Land) (c–d). Temporal evolution of the perturbations for PC1 and PC2. (e–f). April-September sea ice concentration anomaly for PC1+ and PC2+ experiments. Arrows indicate the wind perturbations. Red and blue contours show April-September sea ice anomaly from the observational record regressed on each ZW3 index.

and phase structure of the two leading EOFs of 500 hPa meridional winds (Goyal et al., 2022). The amplitude of the perturbation response is evaluated against the variability over 10 years within the CONTROL simulation.

2.3. Dense Water Formation and Export

Dense water formation is diagnosed using the Surface Water Mass Transformation (SWMT) metric (Abernathey et al., 2016), computed from surface heat and freshwater fluxes. We define the active density classes are defined as SWMT between 30% and 70% of the CONTROL maximum and denser than the SWMT maximum (Schmidt et al., 2025).

10.1029/2025GL119079

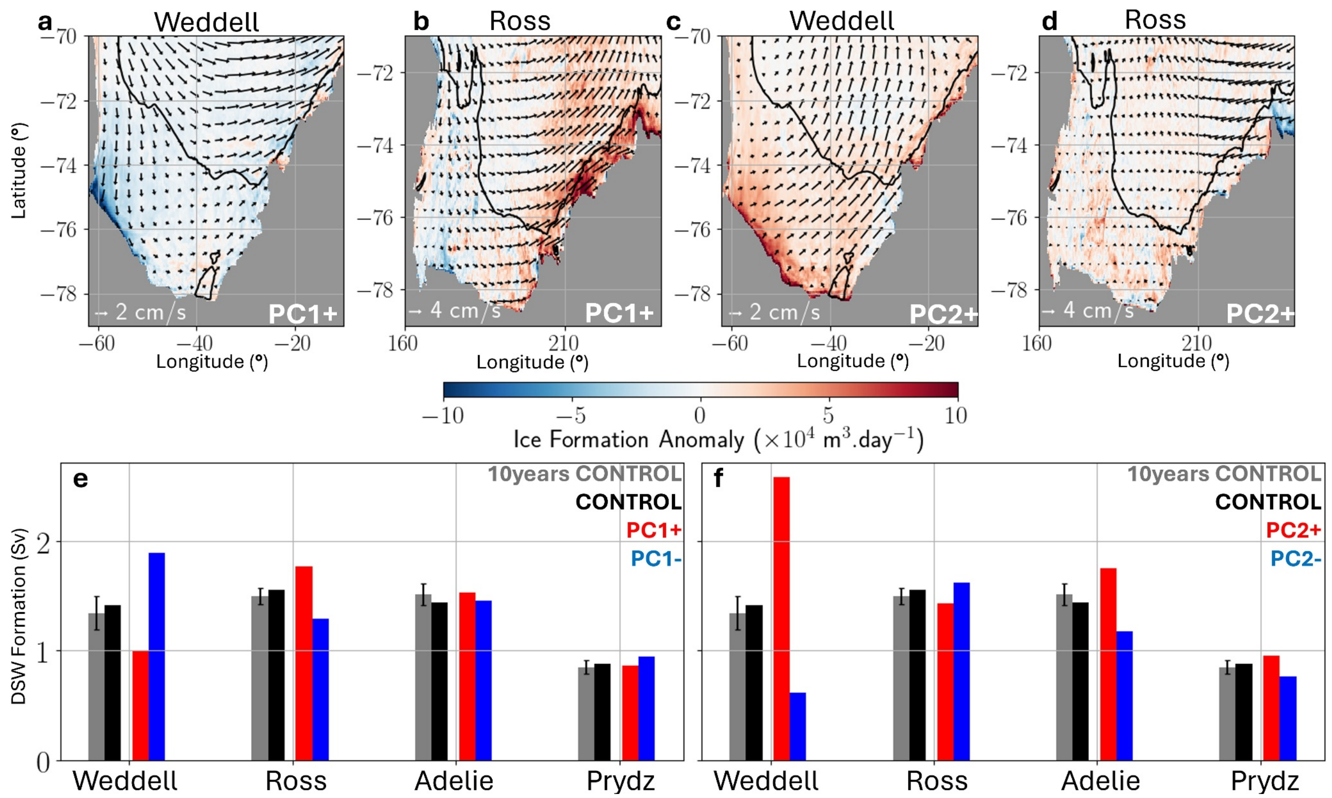

Figure 2. (a–d) The sea ice formation (shading) and sea ice drift (arrows) in the Weddell Sea (a), (c) and Weddell Sea region (b), (d). Panels a and b correspond to the PC1+ case, while (c) and (d) show the PC2+ case. Sea ice formation is calculated as the sum of congelation and frazil ice production, averaged over the first year of the simulation. e-f. Dense water formation on the continental shelf across the four main formation regions, during the first year of perturbation for PC1 (e) and PC2 (f). The black bar represents the CONTROL simulation (a single year in parallel to the perturbations). The gray bar and error bar show the mean formation and standard deviation in the 10 years preceding the perturbation experiment. Red and blue bars show the response to positive and negative perturbations respectively.

Dense water export is measured as transport across the 1000-m isobath, using daily mass fluxes, integrated from the seafloor to $\sigma_1 = 32.56$ kg.m^{-3}, the density of maximum cross-slope transport in ACCESS-OM2 (Auger, Spence, Morrison, Naveira et al., 2025; Morrison et al., 2020).

3. Impact on Sea Ice

The April–September sea ice anomalies in the perturbation experiments closely match observational regressions on each ZW3 principal component (Figures 1e and 1f), confirming realistic sea ice responses. The strongest winter anomalies occur in West Antarctica, particularly in the Ross Sea and western Weddell Sea, aligning with meridional wind anomalies (Figures 1e and 1f). Southward wind anomalies shift the sea ice south, reducing concentration, while northward winds increase it. This asymmetric response has been documented in coupled climate models (Eabry et al., 2024; Goyal et al., 2022) and is known to precondition summer sea ice conditions, contributing to extreme low-ice years (Schroeter et al., 2018).

While the ZW3 mode is the main meridional wind mode over the Southern Ocean, its associated large-scale cyclonic and anticyclonic structures also generate strong zonal winds over the continental shelf (Figures S3 and S4 in Supporting Information S1), leading to enhanced sea ice drift. The perturbations produce coastal sea ice drift anomalies ranging from 1 to 5 cm/s that align well with the expected ZW3 response derived from the observational record (Figure S5 in Supporting Information S1). In the Weddell Sea, wind perturbations also influence sea ice drift near the ice shelf front (Figures 2a and 2c). In the PC1+ simulation, southward winds push sea ice against the western front of the Filchner-Ronne Ice Shelf, suppressing polynya activity and reducing sea ice formation. Conversely, the PC2+ simulation features northward winds across the entire region, opening coastal polynyas along the full ice shelf front (represented as an open water fraction anomaly in Figure S6a in Supporting Information S1), and enhancing sea ice formation. In the PC2+ experiment, the impact on the Ross

Sea is weak because the wind perturbation does not extend far enough south to influence sea-ice drift or formation on the shelf (Figures 1f and 2d). This contrasts with the PC1+ experiment, which does affect the eastern Ross Sea shelf: northeastward drift in the eastern shelf and weaker southeastward drift in the western shelf (Figure 2b). This pattern promotes increased sea ice formation in the eastern Ross Sea due to the enhanced opening of coastal polynyas (Figure S6b in Supporting Information S1).

While ZW3 has a circum-Antarctic structure, its meridional wind anomalies peak in the West Antarctic, Ross and Weddell sectors (Figure 1a and 1b). The meridional wind anomalies are weaker along East Antarctica and only drives minor sea ice drift and formation anomalies in the Prydz Bay and Adélie Land regions (Figure S7 in Supporting Information S1).

4. Impact on Dense Water Formation

ZW3-driven wind anomalies modulate coastal polynyas, affecting DSW formation and subsequent export of bottom water. To evaluate the influence of the perturbation on DSW formation, we focus on the first year of simulation, during the strong ZW3 offset (Figures 2e and 2f). Circumpolar responses are strongest for PC2: PC2+ increases DSW by 13%, PC2− reduces it by 13%, while PC1 effects are weaker (±3%). These circumpolar integrals mask larger regional variations, which become evident when the four main formation regions are examined individually (Figures 2e and 2f). These regional differences are closely linked to changes in sea ice drift and distribution.

4.1. Weddell Sea

Among major DSW regions, the Weddell Sea shows the strongest sensitivity to the ZW3 pattern. In particular, DSW formation is highly sensitive to PC2. PC2+ nearly doubles formation from 1.4 Sv in the CONTROL simulation to 2.6 Sv in the PC2+ experiment (Figure 2f), while PC2− reduces it by half (0.6 Sv). PC1 phases have weaker effects (e.g., 1.0 Sv in PC1−). This strong response to PC2 is linked directly to the extent and direction of the meridional wind perturbations. PC2+ northward winds extend across the entire shelf (Figures 1a and 1b), driving northward sea ice drift over the ice shelf front (Figure 2c), where DSW formation is most active (Figure 3a).

Expanded polynyas in PC2+ enhance ocean–atmosphere heat exchange and sea ice production, strengthening DSW formation. Younger bottom water ages highlight newly formed dense water filling shelf reservoirs and advecting westward, eventually overflowing (Figure 3a). Export of water denser than $\sigma_1 = 32.56$ kg.m^{-3} exceeds 175% of CONTROL, remaining elevated for more than a year after atmospheric forcing returns to normal (Figure 3c). Conversely, PC2− southward wind anomalies lead to sea ice accumulation at the ice shelf front, closing coastal polynyas and reducing DSW formation to half the CONTROL rate (Figure 2f). This suppression has a long-lasting impact on export: DSW outflow continues to decline after the perturbation ends, reaching a minimum of just 0.02 Sv 1.5 years later (Figure 3c). It takes approximately 3 years for DSW export to recover to pre-perturbation levels.

PC1 phases induce weaker but notable export anomalies (up to 50% in PC1−, Figure S8 in Supporting Information S1), as northward winds occur only on the western shelf, producing more localized ice formation (Figures 2a and 2c).

Overall, these perturbation experiments demonstrate that sustained, strong ZW3 events drive multiyear changes in Weddell DSW formation and export. The magnitude of this response significantly exceeds internal variability, as shown by the mean and standard deviation from the 10 years preceding the CONTROL simulation (gray shading, Figure 3c).

While we show that a sustained ZW3 pattern in its PC2 phase can significantly influence DSW formation and export in the Weddell Sea, interannual variability in DSW formation also responds to a combination of large-scale and regional forcings (Zhou et al., 2023). In the historical simulation, the ZW3 mode is embedded within the other forms of atmospheric variability in the JRA55 reanalysis. Nonetheless, we find a low correlation ($r = 0.28$, not significant) between the ZW3 PC2 index and DSW export from the Weddell Sea in the historical simulation, which uses 1958–2018 JRA-55 atmospheric forcing (Figure 3b). This correlation strengthens to $r = 0.50$ (significant at >95%) when the analysis is limited to the 1972–2018 period. The 1958–2018 correlations are weaker than those for 1972–2018 for two main reasons. First, atmospheric reanalysis is poorly constrained by

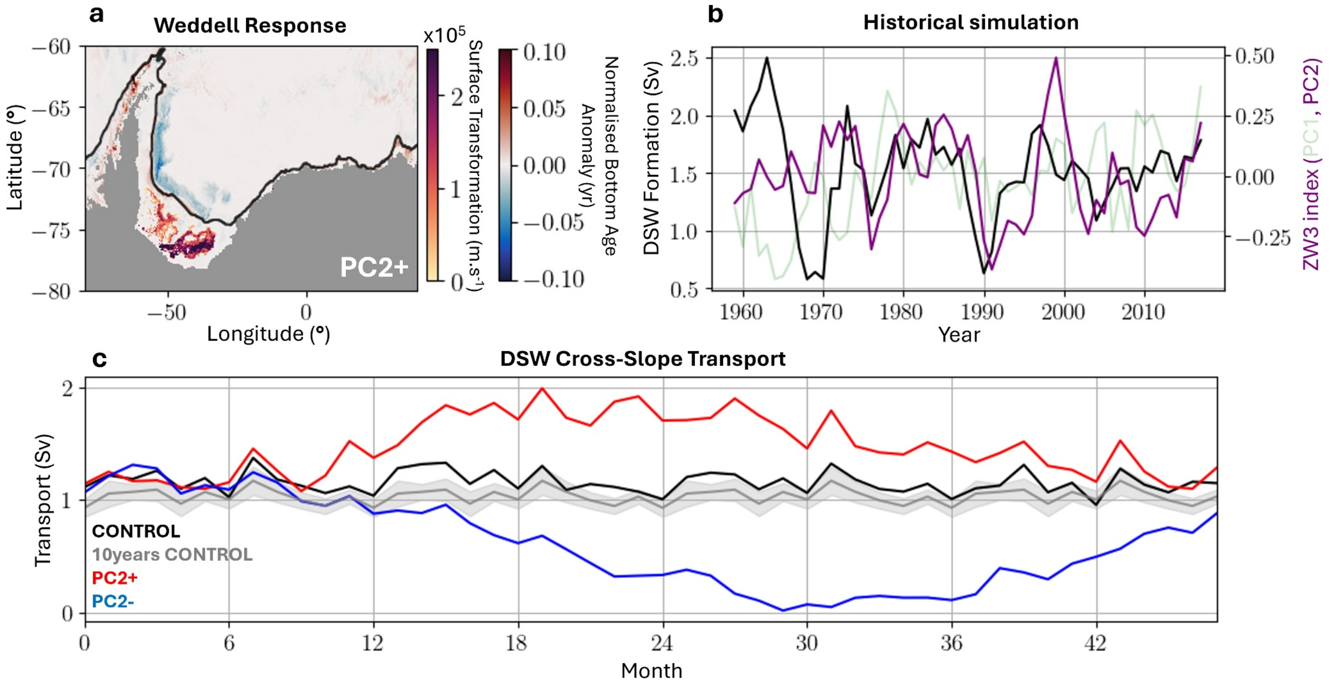

Figure 3. Impacts of a strong Zonal Wave-3 mode with a PC2 phase on the Weddell Sea dense water formation and export. (a) Normalized bottom age anomaly (PC2+ relative to CONTROL) averaged over years 1–2, along with PC2+ surface water mass transformation (SWMT) across $\sigma_0 = [27.81, 27.83]$ kg.m^{-3} on the shelf. (b) Time series of SWMT in the Weddell Sea across $\sigma_0 = [27.81, 27.83]$ kg.m^{-3} from the historical simulation, compared to time series of ZW3 modes PC1 (green) and PC2 (purple) derived from the JRA-55-do reanalysis record. All time series are smoothed using a 3-year running mean. (c) Time series of cross-1000 m isobath transport of water denser that $\sigma_1 = 32.56$ kg.m^{-3} for PC2+ (red), PC2− (blue) and CONTROL (black) experiments. The gray line and error bar show the mean formation and standard deviation in the 10 years preceding the perturbation experiment.

observations before the satellite era (Tsujino et al., 2018). Second, we analyze ACCESS-OM2-01 in its third cycle of 1958–2018 forcing, and each cycle restart causes the forcing to jump unrealistically from 2018 back to 1958, disrupting the model state. Modelers typically discard the initial period after such cycle jumps to allow the model to readjust (Griffies et al., 2014). The correlation is also highest when applying a 3-year running mean, consistent with the multiyear memory of the system seen in our perturbation experiments.

4.2. Ross Sea

In the Ross Sea, PC1+ increases sea-ice formation and DSW production, exceeding one standard deviation of CONTROL variability (Figure 2e). However, the strongest sea ice formation anomaly occurs in the eastern part of the shelf (Figure 2b), while DSW formation is primarily concentrated in the western shelf, particularly in the Terra Nova Bay and Ross Island polynyas (Gordon et al., 2009) (Figure 4a). Still, SWMT responds in the first year, with a 14% DSW formation increase in PC1+, and a 17% reduction in PC1− (Figure 2e). The mechanism leading to more DSW formation is similar the one is described in Schmidt et al. (2025). The perturbation drives increased sea ice formation east of the Ross Sea shelf (200–230°E), due to eastward sea ice drift (Figure 2b). This also translates into younger bottom water age which suggests that newly formed dense water is present (Figure 4a). Salinity anomalies generated in the east propagate westward, reaching 170°E in 50 days, preconditioning the dense water formation regions near Terra Nova Bay (Figure 4b). The salinity at depth in Terra Nova bay responds later in winter, with a 0.05 psμ anomaly between 800 and 900 dbar (Figure 4c). This salinity anomaly is consistent with high salinity anomalies in the observational record of 0.08 psμ (Castagno et al., 2019).

These anomalies allow formation of denser water masses that flood the continental shelf troughs and overflow. The first signal of increased DSW export across the 1000-m isobath appears at the end of the perturbation year (Figure 4d), even though atmospheric forcing has already returned to the CONTROL state. Export increases by 15% over the second year, peaking at 26% in January, and returns to normal by the third year. Both PC1 phases produce anomalies exceeding CONTROL interannual variability (Figure 4d, gray shading).

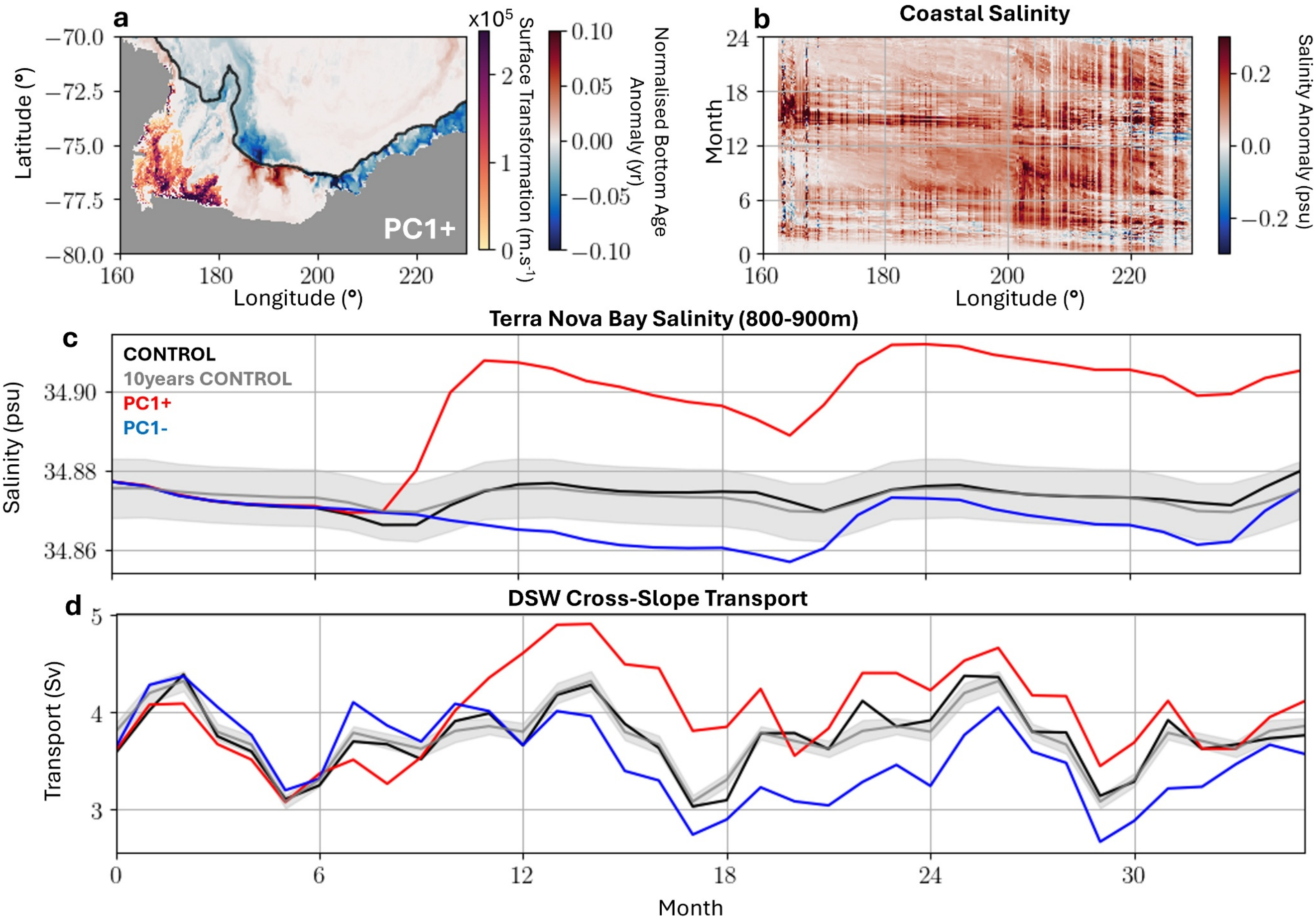

Figure 4. Impacts of a strong Zonal Wave-3 mode with a PC1 phase on the Ross Sea dense water formation and export. (a) Bottom water age anomaly (PC1+ relative to CONTROL) over years 1–2, and mean surface water mass transformation across $\sigma_0 = [27.95, 28.03]$ kg.m^{-3} on the shelf for the PC1+ simulation. (b) Hovmöller diagram of the depth-averaged salinity anomaly during years 1 and 2 as a function of longitude. (c, d). Time series of salinity at 800–900 m depth in Terra Nova Bay. (c) Time series of cross-shelf transport of water denser than $\sigma_1 = 32.56$ kg.m^{-3} for PC1+ (red), PC1− (blue) and CONTROL (black) experiments.

The sensitivity of the Ross Sea to PC1 is further supported by the interannually forced (IAF) simulation: over 1958–2018, the correlation between the ZW3 PC1 index and Ross Sea DSW formation is $r = 0.36$ (with a 3-year running mean applied, significant at 88%). By contrast, the PC2 phase has a minimal influence on the Ross Sea ($r = -0.02$). In the PC2+ experiment, the impact on the Ross Sea is weak, as the wind perturbation does not reach far south enough to impact sea ice drift and formation on the shelf (Figures 1f and 2d), as opposed to PC1+ in the Ross sea eastern shelf. Figure 4 is reproduced for PC2 in Figure S9 in Supporting Information S1.

5. Discussion

We demonstrate that the ZW3 mode significantly influences DSW formation and export around Antarctica. This impact is spatially heterogeneous across major dense water formation sites, with the Weddell Sea showing the strongest sensitivity. Using a high-resolution ocean–sea ice model that accurately reproduces dense water formation in coastal polynyas, we imposed sustained and strong ZW3 perturbations over 1 year and assessed their multiyear impact on DSW export. The response of DSW formation and export varies accordingly to both the phase of the ZW3 mode and the region of formation. The Ross and Weddell Seas exhibit the most marked responses, but they are opposite in sign: ZW3 phases that enhance DSW formation in the Weddell Sea tend to suppress it in the Ross Sea, and vice versa. In the Weddell Sea, strong ZW3 events can either nearly shut down or double DSW export depending on their phase, with effects lasting more than a year after atmospheric forcing returns to normal. The real world response might not be as strong as what is represented by the perturbations applied here. Our perturbation experiments show the response to the upper bound of the sensitivity in a context where the ZW3 pattern perturbation is the only interannual variability forcing. Still, they highlight a sensitivity to this mode which, combined with other climate modes and variability, result in the dense water variability found in the historical simulation. Notably, the signature of this variability is also detectable in the simulation forced by the historical interannual atmospheric record.

Previous studies have identified the role of wind forcing on DSW formation through as the remote wind effect in the Ross Sea (Schmidt et al., 2025; Silvano et al., 2020) at the interannual time scales, or the wind-induced slowdown of DSW export in the Weddell Sea on the multidecadal time scales (Zhou et al., 2023). Our results suggest that the impact of ZW3 mode on DSW formation follows similar dynamics as identified in these previous studies, through a unique climate mode that impacts both region. As the structure of the atmosphere becomes increasingly ZW3-like (Schroeter et al., 2023), the influence of this mode on DSW formation and export is likely to intensify. While the Southern Annular Mode has received much attention in this context, gaining a clearer understanding of ZW3's role completes the picture of how large-scale climate variability affects the Antarctic overturning circulation. Recent work by Eabry et al. (2024) paved the way to understand the joint impact of SAM and ZW3 on sea ice, but effects on the underlying ocean remain largely unstudied. Our results show that ZW3-induced wind and sea ice changes affect the physical processes that form dense water at the Antarctic margins. Moreover, wind and sea ice changes likely influence other oceanic processes—such as warm water intrusions onto the shelf and circulation features in the marginal ice zone. Therefore, ZW3 variability could be an important driver of interannual variability of the circulation of the subpolar Southern Ocean. Its role has likely underappreciated not only due to the historical absence of a phase-resolving index, but also because discussions of Antarctic climate variability have long focused almost exclusively on SAM and ENSO. Recognizing their limitations naturally leads to investigating additional modes such as ZW3.

Finally, accurately representing ZW3 is crucial for simulating trends in abyssal overturning, whose future remains uncertain. Recent work has shown an increasing asymmetry in the Southern Hemisphere atmospheric circulation−a more ZW3-like structure (Schroeter et al., 2023). Currently, trends toward specific ZW3 phases remain unclear. However, accurately capturing the evolution of ZW3, including its teleconnections with tropical variability that help generate the pattern (Goyal et al., 2021), will be crucial for improving projections of future changes in Antarctic Bottom Water formation and global ocean overturning circulation.

Conflict of Interest

The authors declare no conflicts of interest relevant to this study.

Data Availability Statement

0.1°-resolution ACCESS-OM2 Repeat Year Forcing (RYF) and inter-annnual forcing (IAF) model outputs are available in the COSIMA data collection, at https://doi.org/10.4225/41/5a2dc8543105a (Australian National University, 2020). Analysis code is available https://doi.org/10.5281/zenodo.17724474 (Auger, 2025). Processed perturbation simulation outputs used for the analyses of this paper are available at https://doi.org/10.5281/zenodo.17737293 (Auger, Spence, & Morrison, 2025).

Acknowledgments

This research was supported by Australian Research Council (ARC) Discovery Projects DP190100494 and DP250100759, and by the ARC Special Research Initiative, Australian Centre for Excellence in Antarctic Science (SR200100008). The research was undertaken with the assistance of resources and services from the National Computational Infrastructure (NCI), which is supported by the Australian Government. The authors thank the Consortium for Ocean–Sea Ice Modeling in Australia (COSIMA; http://www.cosima.org.au) for making the ACCESS-OM2 configurations available. We also acknowledge the Australian Community Climate and Earth System Simulator National Research Infrastructure (ACCESS-NRI), funded by the Australian Government's National Collaborative Research Infrastructure Strategy, for their maintenance of virtual environments, code and model support. P. S. is supported by ARC Grants FT190100413, CE230100012, DP240102358, LP200100406. Open access publishing facilitated by University of Tasmania, as part of the Wiley - University of Tasmania agreement via the Council of Australian University Librarians.

References

Abernathey, R. P., Cerovecki, I., Holland, P. R., Newsom, E., Mazloff, M., & Talley, L. D. (2016). Water-mass transformation by sea ice in the upper branch of the Southern Ocean overturning. *Nature Geoscience*, *9*(8), 596–601. https://doi.org/10.1038/ngeo2749

Auger, M. (2025). Codes for "the zonal Wave-3 mode impacts antarctic dense water formation [Software]. *Zenodo*. https://doi.org/10.5281/zenodo.17724474

Auger, M., Spence, P., & Morrison, A. (2025b). Data files for the zonal wave-3 mode impacts antarctic dense water formation [Dataset]. *Zenodo*. https://doi.org/10.5281/zenodo.17737293

Auger, M., Spence, P., Morrison, A. K., Naveira Garabato, A., & Silvano, A. (2025c). The variability of Antarctic dense water overflows can be observed from space. *Communications Earth and Environment*, *6*(1), 1–10. https://doi.org/10.1038/s43247-025-02210-7

Australian National University. (2020). COSIMA model output collection [Dataset]. *NCI Australia*. https://doi.org/10.4225/41/5A2DC8543105A

Castagno, P., Capozzi, V., DiTullio, G. R., Falco, P., Fusco, G., Rintoul, S. R., et al. (2019). Rebound of shelf water salinity in the ross sea. *Nature Communications*, *10*(1), 5441. https://doi.org/10.1038/s41467-019-13083-8

Eabry, M. D., Goyal, R., Taschetto, A. S., Hobbs, W., & Gupta, A. S. (2024). Combined impacts of southern annular mode and zonal wave 3 on antarctic sea ice variability. https://doi.org/10.1175/JCLI-D-23-0516.1

Gordon, A. L., Orsi, A. H., Muench, R., Huber, B. A., Zambianchi, E., & Visbeck, M. (2009). Western ross sea Continental slope gravity currents. *Deep Sea Research Part II: Topical Studies in Oceanography*, *56*(13), 796–817. https://doi.org/10.1016/j.dsr2.2008.10.037

Goyal, R., Jucker, M., Gupta, A. S., & England, M. H. (2022). A new zonal Wave-3 index for the southern hemisphere. https://doi.org/10.1175/JCLI-D-21-0927.1

Goyal, R., Jucker, M., Sen Gupta, A., Hendon, H. H., & England, M. H. (2021). Zonal wave 3 pattern in the southern hemisphere generated by tropical convection. *Nature Geoscience*, *14*(10), 732–738. https://doi.org/10.1038/s41561-021-00811-3

Griffies, S. (2012). Elements of the modular ocean model (MOM) (pp. 1–633).

Griffies, S., Yin, J., Durack, P. J., Goddard, P., Bates, S. C., Behrens, E., et al. (2014). An assessment of global and regional sea level for years 1993–2007 in a suite of interannual CORE-II simulations. *Ocean Modelling*, *78*, 35–89. https://doi.org/10.1016/j.ocemod.2014.03.004

Hunke, E., & Lipscomb, W. (2010). CICE: The los alamos sea ice model documentation and software user's manual version 4.0 LA-CC-06-012. *Tech. Rep. LA-CC-06-012*.

Jena, B., Kshitija, S., Bajish, C. C., Turner, J., Holmes, C., Wilkinson, J., et al. (2024). Evolution of Antarctic sea ice ahead of the record low annual maximum extent in September 2023. *Geophysical Research Letters*, *51*(7), e2023GL107561. https://doi.org/10.1029/2023GL107561

Kiss, A. E., Hogg, A. M., Hannah, N., Boeira Dias, F., Brassington, G. B., Chamberlain, M. A., et al. (2020). ACCESS-OM2 v1.0: A global ocean–sea ice model at three resolutions. *Geoscientific Model Development*, *13*(2), 401–442. https://doi.org/10.5194/gmd-13-401-2020

Meehl, G. A., Arblaster, J. M., Chung, C. T. Y., Holland, M. M., DuVivier, A., Thompson, L., et al. (2019). Sustained ocean changes contributed to sudden antarctic sea ice retreat in late 2016. *Nature Communications*, *10*(1), 14. https://doi.org/10.1038/s41467-018-07865-9

Mensah, V., Nakayama, Y., Fujii, M., Nogi, Y., & Ohshima, K. I. (2021). Dense water downslope flow and AABW production in a numerical model: Sensitivity to horizontal and vertical resolution in the region off cape darnley polynya. *Ocean Modelling*, *165*, 101843. https://doi.org/10.1016/j.ocemod.2021.101843

Morales Maqueda, M. A., Willmott, A. J., & Biggs, N. R. T. (2004). Polynya dynamics: A review of observations and modeling. *Reviews of Geophysics*, *42*(1). https://doi.org/10.1029/2002RG000116

Morrison, A. K., Hogg, A. M., England, M. H., & Spence, P. (2020). Warm circumpolar deep water transport toward Antarctica driven by local dense water export in canyons. *Science Advances*, *6*(18), eaav2516. https://doi.org/10.1126/sciadv.aav2516

Nihashi, S., & Ohshima, K. I. (2015). Circumpolar mapping of antarctic coastal polynyas and landfast sea ice: Relationship and variability. *Journal of Climate*, *28*(9), 3650–3670. https://doi.org/10.1175/JCLI-D-14-00369.1

Purich, A., England, M. H., Cai, W., Sullivan, A., & Durack, P. J. (2018). Impacts of broad-scale surface freshening of the Southern Ocean in a coupled climate model. *Journal of Climate*, *31*(7), 2613–2632. https://doi.org/10.1175/JCLI-D-17-0092.1

Purich, A., & England, M. H. (2019). Tropical teleconnections to antarctic sea ice during Austral spring 2016 in coupled pacemaker experiments. *Geophysical Research Letters*, *46*(12), 6848–6858. https://doi.org/10.1029/2019GL082671

Raphael, M. N. (2004). A zonal wave 3 index for the southern hemisphere. *Geophysical Research Letters*, *31*(23). https://doi.org/10.1029/2004GL020365

Schlosser, E., Haumann, F. A., & Raphael, M. N. (2018). Atmospheric influences on the anomalous 2016 antarctic sea ice decay. *The Cryosphere*, *12*(3), 1103–1119. https://doi.org/10.5194/tc-12-1103-2018

Schmidt, C., Morrison, A. K., & England, M. H. (2023). Wind– and sea-Ice–Driven interannual variability of Antarctic bottom water formation. *Journal of Geophysical Research: Oceans*, *128*(6), e2023JC019774. https://doi.org/10.1029/2023JC019774

Schmidt, C., Morrison, A. K., England, M. H., & Silvano, A. (2025). *West antarctic melt variability and wind anomalies contribute to ross sea salinity rebound*. ESS Open Archive. https://doi.org/10.22541/essoar.173870875.51711851/v1

Schroeter, S., Hobbs, W., Bindoff, N. L., Massom, R., & Matear, R. (2018). Drivers of antarctic sea ice volume change in CMIP5 models. *Journal of Geophysical Research: Oceans*, *123*(11), 7914–7938. https://doi.org/10.1029/2018JC014177

Schroeter, S., O'Kane, T. J., & Sandery, P. A. (2023). Antarctic sea ice regime shift associated with decreasing zonal symmetry in the southern annular mode. *The Cryosphere*, *17*(2), 701–717. https://doi.org/10.5194/tc-17-701-2023

Silvano, A., Foppert, A., Rintoul, S. R., Holland, P. R., Tamura, T., Kimura, N., et al. (2020). Recent recovery of Antarctic Bottom Water formation in the ross sea driven by climate anomalies. *Nature Geoscience*, *13*(12), 780–786. https://doi.org/10.1038/s41561-020-00655-3

Stewart, K. D., Kim, W. M., Urakawa, S., Hogg, A. M., Yeager, S., Tsujino, H., et al. (2020). JRA55-do-based repeat year forcing datasets for driving ocean–sea-ice models. *Ocean Modelling*, *147*, 101557. https://doi.org/10.1016/j.ocemod.2019.101557

Tsujino, H., Urakawa, S., Nakano, H., Small, R. J., Kim, W. M., Yeager, S. G., et al. (2018). JRA-55 based surface dataset for driving ocean–sea-ice models (JRA55-do). *Ocean Modelling*, *130*, 79–139. https://doi.org/10.1016/j.ocemod.2018.07.002

Wang, G., Hendon, H. H., Arblaster, J. M., Lim, E.-P., Abhik, S., & van Rensch, P. (2019). Compounding tropical and stratospheric forcing of the record low Antarctic sea-ice in 2016. *Nature Communications*, *10*(1), 13. https://doi.org/10.1038/s41467-018-07689-7

Zhou, S., Meijers, A. J. S., Meredith, M. P., Abrahamsen, E. P., Holland, P. R., Silvano, A., et al. (2023). Slowdown of Antarctic bottom water export driven by climatic wind and sea-ice changes. *Nature Climate Change*, *13*(7), 1–9. https://doi.org/10.1038/s41558-023-01695-4